ACS APPLIED MATERIALS & INTERFACES

Research Article

www.acsami.org

Microfluidic Synthesis of Monodisperse Nanoporous Oxide Particles and Control of Hierarchical Pore Structure

Nick J. Carroll,[†,‡] Peter F. Crowder,[†,‡] Svitlana Pylypenko,[†,§] Wendy Patterson,[†,§] Dilru R. Ratnaweera,[⊥] Dvora Perahia,[⊥] Plamen Atanassov,[†,‡,§] and Dimiter N. Petsev*[,†,‡,§]

[†]Department for Chemical and Nuclear Engineering and [§]Center for Emerging Energy Technologies and [‡]Center for Biomedical Engineering, University of New Mexico, Albuquerque, New Mexico 87131, United States

[⊥]Department of Chemistry, Clemson University, Clemson, South Carolina 29634, United States

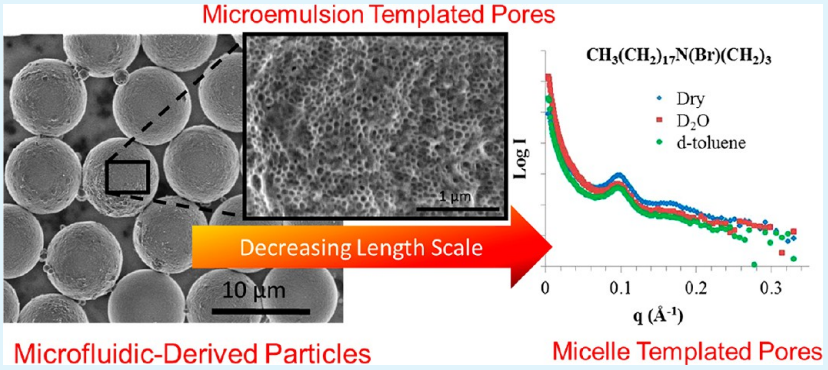

ABSTRACT: Particles with hierarchical porosity can be formed by templating silica microparticles with a specially designed surfactant micelle/oil nanoemulsion mixture. The nanoemulsion oil droplet and micellar dimensions determine the pore size distribution: one set of pores with diameters of tens of nanometers coexisting with a second subset of pores with diameters of single nanometers. Further practical utility of these nanoporous particles requires precise tailoring of the hierarchical pore structure. In this synthesis study, the particle nanostructure is tuned by adjusting the oil, water, and surfactant mixture composition for the controlled design of nanoemulsion-templated features. We also demonstrate control of the size distribution and surface area of the smaller micelle-templated pores as a consequence of altering the hydrophobic chain length of the molecular surfactant template. Moreover, a microfluidic system is designed to process the low interfacial system for fabrication of monodisperse porous particles. The ability to direct the assembly of template nanoemulsion and micelle structures creates new opportunities to engineer hierarchically porous particles for utility as electrocatalysts for fuel cells, chromatography separations, drug delivery vehicles, and other applications.

KEYWORDS: *porous particles, microfluidics, nanoemulsion, sol gel, silica, micelle*

INTRODUCTION

New strategies for synthesis of particles with controllable nanostructure provide opportunities for application-directed tailoring of structural design. A material of particular interest is a collection of nanoporous particles;[1−3] they have utility as vehicles for targeted drug delivery and in biomolecular[4] and cellular encapsulation[5,6] applications. A powerful fabrication method for nanoporous particles is preservation of self-assembled surfactant micelle structures in aqueous drops of soluble silica species by means of sol gel chemistry.[7] However, these particles are limited to pores with diameters of a few nanometers and often enclose porous structures rendered inaccessible at the particle surface due to formation of a solid material layer at the surface.[8,9] Recently we have reported on the sol−gel synthesis of silica particles with hierarchical pore size[10] obtained through evaporative-induced solidification (EIS) of micrometer-size aqueous polymer precursor drops encasing nanoemulsion[11−15] and surfactant micelle templates. Nanoemulsion droplets act as templates for pores with diameters of tens of nanometers, whereas self-assembled surfactant micelle structures act as templates for a smaller subset of pores, with diameters of single nanometers.[16] The larger pores confer cargo diversity to the particles; they allow for loading of larger molecules and colloids within the porous matrix than is possible with porous particles formed solely through surfactant self-assembly. The functionality of our particles is further enhanced by pore structures that are accessible at the particle surface. This connectivity is illustrated by their use as templates for replica electrocatalyst materials[10,17] and high-surface-area scaffolds for lipid-based drug delivery vehicles.[18,19] However, further practical utility of these

Received: May 20, 2012
Accepted: February 6, 2013
Published: February 6, 2013

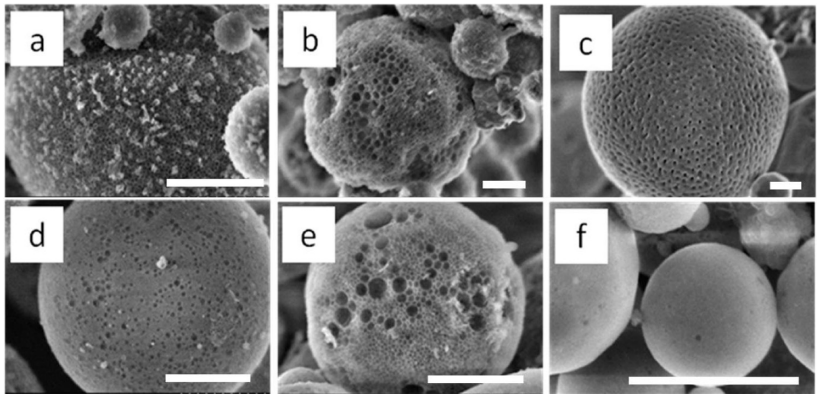

Figure 1. SEM micrographs of particle surfaces prepared using (a) standard sol, (b) addition of 0.075 M NaCl, (c) addition of 0.15 M NaCl, (d) 2:1 oil to sol ratio, (e) 25% less ABIL EM90 surfactant, (d) 25% increase in CTAB surfactant. All scale bars are 1 μm.

nanoporous particles requires tailoring of pore structure for specific applications.

Better understanding of the oil/water/surfactant mixture that governs the hierarchical pore structure will enable the next generation of porous materials through controlled design. For example, structural design of the larger subset of pores with diameters of tens of nanometers could be achieved by tuning of the nanoemulsion phase through component mixture variation. However, for many applications, tailoring of the smaller micelle templated pores (single nanometers) is the essential design feature. For example, a goal of modern catalysis is to reduce the loading of noble metals while maintaining a high surface area and activity. In this regard, design of the smaller micelle-templated pores is critical; the pore size distribution determines the size and dispersion of noble metal colloids grown within the porous structures.[20,21]

Design at a much larger length scale is afforded by the recent advancements in microfluidics, providing a powerful tool for processing oil/water/surfactant systems to generate monodisperse precursor drops and hence resultant microparticles.[22−26] This is a significant advantage oversimple mechanical stirring of oil, water, and surfactant mixtures which usually results in polydisperse drop size distributions.[27−31] However, the applicability of drop microfluidics to low interfacial tension systems is limited because precursor drops characterized by small Laplace pressures are easily ruptured and thus require mild processing conditions. Therefore, in addition to investigation of nanopore formation through mixture variation, there remains a need for enhanced microfluidic design for mild processing of preparticle drops.

In this fabrication study, we investigate component mixture variation effect on the nanostructure of the resultant porous particles. The surfactant, electrolyte, and water/oil ratios are varied to determine the effect on the formation of nanoemulsion templated features. We demonstrate control over pore size and surface area of the smaller, micelle templated pores as a consequence of altering chain length of the molecular surfactant template. In addition, porous particles with a narrow size distribution are formed by EIS processing of microfluidic-derived prepolymer drops at mild, ambient conditions. The formation of hierarchal bicontinuous open structured pores enhanced by narrow size particle distribution represents a major advancement in templating of nanomaterials with well-controlled properties. The resultant nanoporous structures are characterized using a combination of techniques including X-ray diffraction (XRD), small angle neutron scattering (SANS), scanning electron microscopy (SEM), and physisorption analysis for pore size distribution and surface area.

EXPERIMENTAL SECTION

To fabricate silica particles with hierarchical pore structure, a standard aqueous precursor recipe is prepared by dissolving 1.82 g of cetyltrimethylammonium bromide (CTAB, Sigma) in 20 g of deionized water under vigorous stirring at 40 °C until the solution is clear. Next, 5.2 g of tetraethyl orthosilicate (TEOS, Sigma) (Purum >98%) and 0.57 g of 1 N hydrochloric acid (HCl) are added to the mixture under vigorous stirring at room temperature for 30 min to hydrolyze and dissolve the TEOS monomer. The oil phase is prepared by dissolving a modified polyetherpolysiloxane/dimethicone copolyol surfactant with the trade name ABIL EM 90 (Degussa) in hexadecane (3 wt %). To fabricate particles for the investigation of mixture variation on the resultant pore structures, we used a bulk emulsification strategy; the prepared aqueous silica precursor mixture is added to the oil phase and shaken vigorously to produce an emulsion. The emulsion is transferred to a 1000 mL round-bottom flask and heated to 80 °C under a reduced pressure of 9.3 Pa for 3 h. The resultant particles are segregated by centrifugation, the continuous oil phase is removed, and the particles are calcined in air at 500 °C for 5 h to replace the organic templates with air. To study alterations of the particle nanostructure as a consequence of modification to the nanoemulsion phase, we alter the mixture by varying oil to water ratios, electrolyte concentration and surfactant concentration; deviations from the standard recipe are described in the text. The effect of surfactant molecular weight on the size distribution of micelle templated pores is examined by varying the length of the hydrophobic block of the cationic trimethyl ammonium bromide surfactant template from C13 to C19. To demonstrate formation of monodisperse aqueous precursor drops and hence microparticles, we use polydimethysiloxane (PDMS, Dow Corning) microfluidic channels (height and width of 10 μm) fabricated by soft lithography[32] methods. The silica precursor drops in hexadecane oil are formed by supplying the aqueous and organic oil phases into a microfluidic device using two digitally controlled Harvard Pico Plus syringe pumps. The aqueous precursor is flow-focused and consequently controllably emulsified into drops by the viscous flow of the immiscible oil phase within the orifice of a T-shaped microfluidic device.[33] The volumetric flow rate for the aqueous precursor is 0.1 μL/min, with 1 μL/min being a typical flow rate for the continuous oil phase. The precursor drops are then collected in a 6 mm diameter reservoir and the solvent is evaporated from the drops at ambient conditions to consolidate them into solid particles.

X-ray diffraction (XRD) measurements are performed on an automated X-ray powder diffractometer (Scintag, Pad V). The X-ray radiation is obtained by use of a long line focus copper X-ray tube powered at 800W. The Cu Kα radiation (λ = 1.54 Å) is separated from the β line using a Nickel foil filter. The data acquisition angular range

2θ is varied between 1 and 5°, in a step scanning mode with a step size of 0.05° and dwell time of 20 s. Surface area and pore size distribution data are obtained on a Micromeritics Gemini pycnometer, which uses the static volumetric technique to generate high speed surface area and porosity data. Brunauer–Emmett–Teller (BET) surface areas are estimated from nitrogen adsorption measurements at 77.4K, after the samples were outgassed overnight at 120 °C under a nitrogen environment. Relative standard deviations for single-point BET measurements are less than 1%. Scanning electron microscopy (SEM) was done on a Hitachi S-800 instrument.

Small-angle neutron scattering experiments are carried out on the Low Q Diffractometer (LQD), FP10 beamline in Lujan Center at Los Alamos National Laboratory. LQD covers the wavelength range of 1.5 to 15 Å with the q range of 0.003 to 0.5 $Å^{-1}$ where q is the momentum transfer, given by $q = 4\pi\sin(\theta)/\lambda$, θ is the angle of incidence and λ is the wavelength of the radiation. Background, empty cell, water, and toluene are measured separately and subtracted from the data. The data are then normalized to the transmission of the samples.

RESULTS AND DISCUSSION

Mixture Component Variation Effect on Particle Structure. It has been determined that slight variations in nanoemulsion mixture components (electrolyte concentration, wt % surfactants, oil to sol ratio, etc.) can produce strikingly different pore morphologies and particle surface areas. This outcome is not surprising as variations in electrolyte concentration and surfactant concentrations have direct effect on interfacial tension which determines the type and phase structure of nanoemulsion formed.[34] Figure 1 shows SEM images representative of the various particle surface morphologies formed due to variations in the nanoemulsion mixture components. The standard nanoemulsion recipe is used as in previous work[10] and particles are formed with surface cavities (30–40 nm) in a honeycomb-like morphology (Figure 1a) with a BET surface area of 1000 ± 10 m^2/g. The molar ratios for the standard recipe sol were $TEOS/H_2O/HCl/CTAB$ = 1:44.5:0.63:0.20, with no added electrolytes. The oil phase consists of 3 wt % Abil EM-90 in hexadecane. Sol to oil phase ratio is 1:3.

Addition of NaCl (either 0.075 or 0.15 M NaCl) to the standard sol mixture results in formation of particles with lower BET surface area (650 and 850 m2/g, respectively) and deviation from the evenly distributed "honeycomb" morphology of the standard material (Figure 1b, c). Reducing the sol to oil ratio (1:2) results in formation of particles with less open structure but BET surface area similar to that of the standard material (1038 m2/g) (Figure 1d). Reducing the concentration of oil phase surfactant, Abil Em-90, by 25% produced material with BET surface area similar to the standard material (975 m^2/g), but with a more open structure; here, in addition to "honeycomb"-like openings, larger spherical cavities are also observed. The larger surface cavities observed throughout the sample may be due to nanoemulsion droplet coalescence related to lower emulsifying surfactant concentrations at elevated temperature. Increasing concentration of water-soluble CTAB surfactant leads to an increase in the BET surface area (1250 m^2/g) and the disappearance of the honeycomb open structure (Figure 1f). Both of these factors indicate formation of pores that are more similar to those formed exclusively with CTAB micelles in the absence of nanoemulsion droplets.

Size Control of Pores Templated by Micelles. To investigate the tailoring of micelle-templated pores, the length of the hydrocarbon block of the cationic trimethyl ammonium bromide template surfactant is varied while maintaining component concentrations and processing conditions as described in the standard precursor recipe. Increasing the length of the hydrocarbon block of the template surfactant by one ethyl group results in decrease in surface area by 13% (down to 873 m^2/g); by contrast, decreasing the length of the hydrocarbon block by one ethyl group increases the surface area by 13% (up to 1136 m^2/g). Further decrease in the surfactant length by yet another ethyl group leads to further increase in surface area, up to 1198 m^2/g. The XRD data of the resultant particles in Figure 2 show that reducing the length of

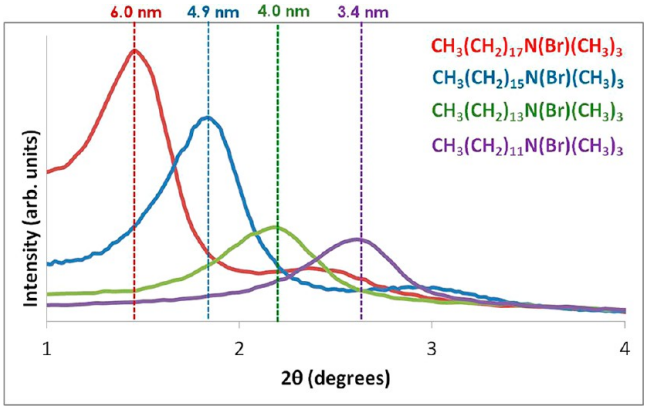

Figure 2. XRD data for mesoporous silica particles. Progressively reducing the hydrocarbon block of the cationic templating surfactant leads to a reduction in the d-spacing and pore size of the micelle-templated pores.

the hydrocarbon chain progressively by one ethyl group produces porous structures of decreasing size, from 6 to 3.4 nm, as determined by the XRD d-spacing. Interestingly, while the pore size distribution is altered by adjusting the hydrophobic block length of the templating surfactant, we observe no changes to the morphology of the larger pores templated by the oil nanoemulsion phase.

Small-angle neutron scattering (SANS) studies are carried out on dry microparticles made with surfactants with chain length varying from C13 to C19. The results for dry particles and particles immersed in water and toluene are shown in Figure 3. The patterns consist of a broad peak centered at the mean size of the pores with width corresponding to the size distribution. The peak positions are determined by $d \sim 2\pi/q$ for small angles, and the dimensions obtains are similar to those measured by XRD in Figure 2. With increasing chain length, the peak shifts to lower q values as the pores become larger. The line widths of the peaks decrease and higher order lines are observed as the chain length of the surfactant is increased and the distribution of pore size decreases. Scattering at low q is indicative of larger structures that persist across the samples. These, however, are not well-defined. These observations are consistent with the microscopy results.

The formation of particles with surface accessible, interconnected pores is substantiated by immersing the samples in solvents and following the SANS patterns; here, the two types of solvents utilized are water and toluene. Representative patterns are shown in Figure 3. The obtained SANS patterns follow those of the dry particles, indicating that the formed porous structures remain stable. However, small differences were observed in the intensity of the lines. These differences correspond to enhanced contrast formed by the solvents penetrating the matrix. This intensity difference is consistent

dx.doi.org/10.1021/am3030195 | ACS Appl. Mater. Interfaces 2013, 5, 3524–3529

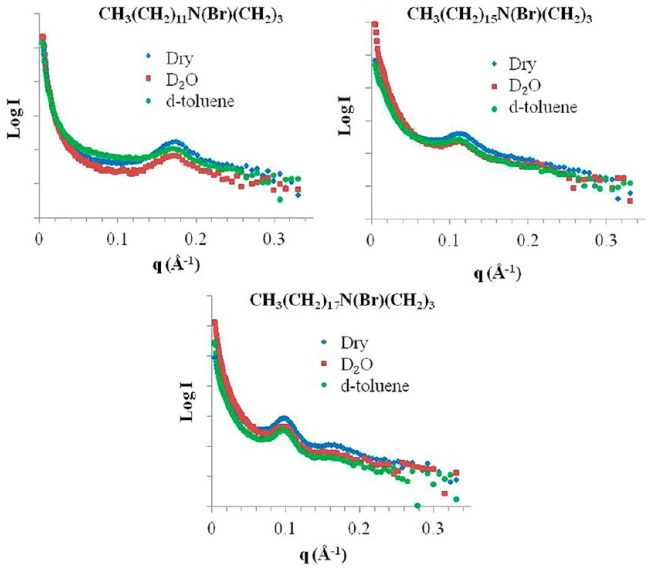

Figure 3. Small angle neutron scattering in terms of log I as a function of momentum transfer q, normalized to background and solvents, of porous particles made by surfactants with the indicated chain length. Blue symbols correspond to the dry particles, red to D_2O and green to d-toluene.

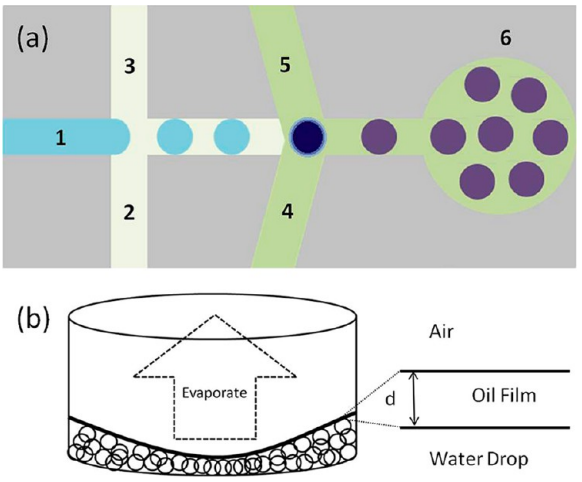

Figure 4. (a) Microfluidic configuration. Aqueous silica precursor (1) is emulsified in a 10 μm diameter orifice with pure hexadecane oil (2, 3). Drops travel down the 10 μm diameter channel where hexadecane with 2 wt % Abil EM90 surfactant (4, 5) is added allowing the nanoemulsion phase to form and penetrate the aqueous silica precursor drops. (b) The drops are collected in a reservoir (6 mm diameter) where EISA is carried out at ambient pressure and temperature; oil is removed to minimize diffusion oil film and increase evaporation flux.

with connected pores as indicated by the low angle scattering. These SANS measurements show that the solvent occupies all sites within the particles, where both hydrophilic and hydrophobic substances can reside within the pores. The results of this investigation illustrate the promise of tailored structural design of the smaller pores through control of templating surfactant chain length; this can be of particular interest for designing porous particles for the templating of supported noble metal catalyst materials or creating high-surface-area scaffolds for drug delivery vehicles.

Drop Microfluidics for Fabrication of Particles with Narrow Size Distribution. The low interfacial tension necessary to form the oil nanoemulsion phase within our aqueous silica precursor drops makes integration of drop formation within a microfluidic device difficult. This is demonstrated by the characteristic time (τ) to reach capillary instability[35]

$$\tau \approx \frac{\mu r}{\gamma} \quad (1)$$

where μ is fluid stream viscosity, r is the drop radius, and γ is the interfacial tension. Thus as interfacial tension becomes very small, the time for thread instability and breakage into drops within the microfluidic orifice approaches infinity. To circumvent this problem, the precursor aqueous drops are initially formed in a pure hexadecane oil phase within a microfluidic device orifice and subsequently a surfactant-laden oil solution is injected downstream of the orifice as described by the schematic in Figure 4a. The stream of aqueous silica precursor prepared from the standard recipe (channel 1) is emulsified in a 10 μm diameter orifice with pure hexadecane oil (channels 2 and 3). The drops travel downstream and are physically separated by the pure oil phase which prevents interaction and coalescence. Next, hexadecane with 2 wt % Abil EM90 surfactant (channels 4 and 5) is injected into the stream. This lowers the interfacial tension to initiate the formation of nanoemulsion droplets, which then penetrate into interior of the aqueous silica precursor drops. The drops are then collected in a 6 mm diameter reservoir (6). Thereafter, the water solvent and silicate reaction byproduct ethanol are evaporated out of the silica precursor drops to induce gelation and drive surfactant self-assembly.[9,10,36]

In our previous nanoemulsion-templated silica particle synthesis experiments,[10] emulsion evaporation was carried out at an elevated temperature of 80 °C under vacuum pressure; vigorous bubbling was observed during this evaporation process. However, to form monodisperse particles, it is necessary to avoid vigorous bubbling of the emulsion to minimize shearing of the fragile silica precursor drops.

Therefore, emulsion evaporation for monodisperse particle synthesis is carried out at ambient temperature and pressure to avoid vigorous bubbling and drop disruption. Aranberri[37] and co-workers determined that emulsion drop evaporation occurs through a mechanism whereby the drops remain separated from the vapor phase by a liquid continuous phase film; transport of solvent from the drops to the vapor phase occurs by diffusion of dissolved molecules through the continuous phase film. It was determined that the flux J across the continuous phase is related to the linear concentration gradient:

$$J = D\frac{C_s - C_I}{d} \quad (2)$$

where D is the diffusion coefficient of drop solvent in the continuous phase, C_s is the concentration of solvent at the drop surface, C_I is the concentration of drop solvent at the continuous phase/vapor interface, and d is the thickness of the continuous phase film. Thus, to increase the flux of solvent from the drops for particle synthesis, most of the hexadecane oil phase is removed by pipetting until only a thin film (d) remains above the gravity-settled aqueous precursor drops as shown schematically in Figure 4b.

An optical micrograph of the resultant silica precursor drops in the collection reservoir is shown in Figure 5a. Opaqueness forms in the continuous phase near the drops, which makes

dx.doi.org/10.1021/am3030195 | ACS Appl. Mater. Interfaces 2013, 5, 3524−3529

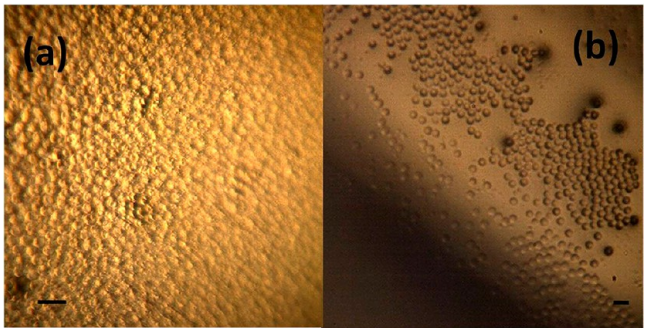

Figure 5. (a) Aqueous silica precursor drops in hexadecane oil phase. Opaqueness is observed in the continuous phase near the drops (scale bar 20 μm). (b) Silica particles in hexadecane oil phase after evaporative processing in collection reservoir (scale bar 15 μm).

clear imaging of the drops difficult. This opaqueness was also observed in previous synthesis experiments using a bulk emulsion.[10] Following evaporative processing of the precursor drops, the resultant silica particles are imaged within the reservoir using optical microscopy as shown in Figure 5b. The particles are subsequently washed with hexane and dried; the microfluidic-derived particles are imaged using SEM as shown in Figure 6a, with higher magnification image shown in Figure 6b. Smaller particles are also observed throughout the sample as highlighted by the arrows in the SEM image in Figure 6c. These smaller particles are attributed to the formation of satellite drops[33] during emulsification in the microfluidic orifice or shearing of the drops as they exit the device into the collection reservoir. A few larger particles are also observed in the sample as highlighted by the circled particle in Figure 6c; these particles are most likely formed because of coalescence of drops before evaporative processing proceeds to completion. The quantification of the size distribution of our particles is achieved using TIFF images from SEM analysis. A total of 400 particles were collected and analyzed using ImageJ software to measure the particle diameters; the resultant size distribution graph is shown in Figure 6d. The mean particle size is estimated to be 7.7 μm with standard deviation of 1 μm. For comparison, the size distribution and representative SEM image of more polydisperse particles synthesized using a bulk emulsion are shown in Figure 6e; here, the mean particle size is 1.2 μm with standard deviation of 1.1 μm.

The obtained silica particles exhibit a honeycomb-like surface structure as observed by the SEM images shown in panels a and b in Figure 6; this is in excellent agreement with the surface morphology observed for porous particles formed by nanoemulsion and surfactant templating using the standard recipe and bulk emulsification technique. Thus, by using a drop-based microfluidic approach and mild evaporative processing conditions, we demonstrate the fabrication of porous particles with a markedly improved size distribution in comparison to particles formed through a bulk emulsification strategy. The microfludic derived particles still have strikingly similar pore morphology (see Figure 7a, b) as those obtained in the batch samples (see Figure 1a).

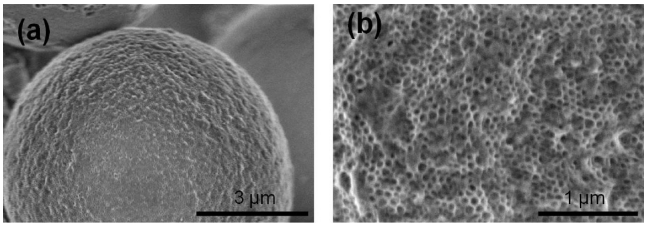

Figure 7. (a, b) SEM micrographs showing the honeycomb-like surface morphology of microfluidic-derived porous particles.

CONCLUSION

We have demonstrated the fabrication versatility of hierarchically nanostructured silica particles through controlled design of nanoemulsion and micellar phase templating. For the multimodal nanoporous particles presented herein, we have determined that variation of the nanoemulsion mixture components provides a powerful tool for the tuning of the

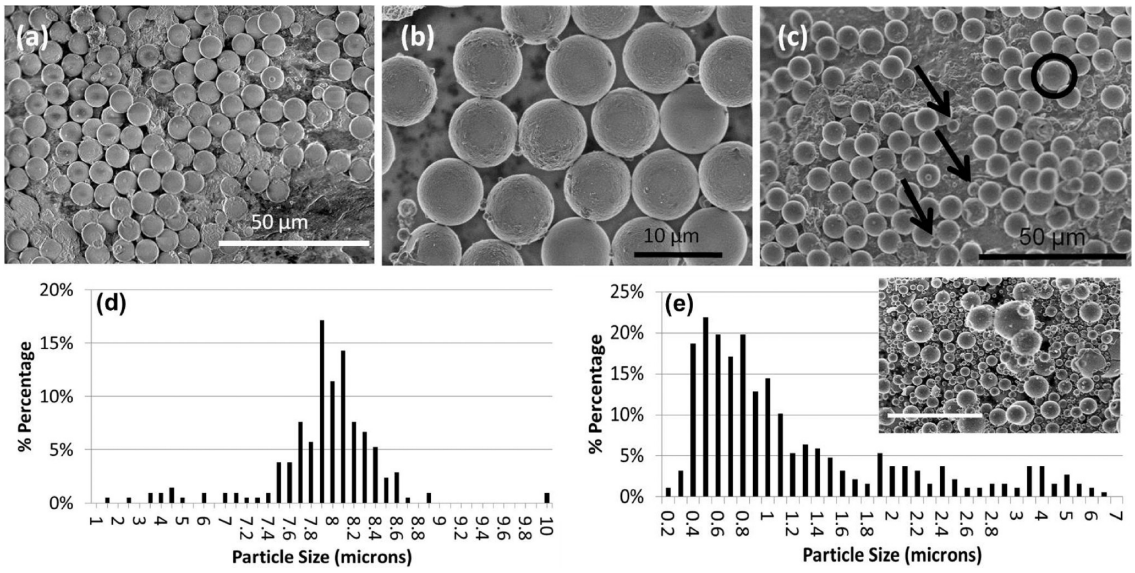

Figure 6. (a, b) SEM images of monodisperse nanoemulsion-templated silica particles. (c) SEM micrograph shows existence of small particles (arrows) due to satellite drop formation or shearing and large particles due to drop coalescence (circle). (d) Size distribution graph of microfluidic-derived particles. (e) Size distribution graph of particles derived from bulk emulsion; inset: SEM image of the resultant particles (scale bar is 10 μm).

dx.doi.org/10.1021/am3030195 | ACS Appl. Mater. Interfaces 2013, 5, 3524−3529

particle nanostructure. Additionally, the ability to reproducibly alter the template liquid structures formed by surfactant micelle construction has been shown to be a key element in providing yet another level of design control; for example, the tailoring of micelle-templated pore size and surface area by altering the surfactant hydrocarbon block length.

A specially designed drop-based microfluidics approach has been developed that allows for formation of monodisperse silica particles with hierarchical porosity. Emulsification of silica precursor in a pure oil phase at the microfluidic orifice, with infusion of surfactant-laden oil phase into the device downstream of the orifice, allows for facile microfluidic processing of a low interfacial tension system. Temperate evaporation of the solvent from the drops at ambient conditions preserves the size distribution of the fluidic-formed silica precursor drops during gelation.

We present a pragmatic approach to achieve control at three different length scales: the nanoscale via surfactant micelle templating, the tens of nanometers via nanoemulsion phase templating, and at the micrometer scale through control of overall size distribution by processing polymer precursor drops within a microfluidic platform. Our results may be useful to help guide the process of designing porous particles for specific function, thus further enhancing the promise of these particles for practical application.

AUTHOR INFORMATION

Corresponding Author

*E-mail: dimiter@unm.edu.

Notes

The authors declare no competing financial interest.

ACKNOWLEDGMENTS

This work was supported by NSF (PREM/DMR 0611616), NSF (CBET 0828900), DoE-EPSCoR Implementation Program: Materials for Energy Conversion. We thank Gabriel Lopez for helpful advice and stimulating scientific discussion related to this work. We thank Danielle Lussier for Figure 4a.

REFERENCES

(1) Rao, G. V. R.; Lopez, G. P.; Bravo, J.; Pham, H.; Datye, A. K.; Xu, H. F.; Ward, T. L. *Adv. Mater.* **2002**, *14*, 1301−1304.
(2) Yu, M. H.; Zhou, L.; Zhang, J.; Yuan, P.; Thorn, P.; Gu, W. Y.; Yu, C. Z. *J. Colloid Interface Sci.* **2012**, *376*, 67−75.
(3) Dragosavac, M. M.; Vladisavljevic, G. T.; Holdich, R. G.; Stillwell, M. T. *Langmuir* **2012**, *28*, 134−143.
(4) Luo, T. J. M.; Soong, R.; Lan, E.; Dunn, B.; Montemagno, C. *Nat. Mater.* **2005**, *4*, 220−224.
(5) Chia, S. Y.; Urano, J.; Tamanoi, F.; Dunn, B.; Zink, J. I. *J. Am. Chem. Soc.* **2000**, *122*, 6488−6489.
(6) Kaehr, B.; Townson, J. L.; Kalinich, R. M.; Awad, Y. H.; Swartzentruber, B. S.; Dunphy, D. R.; Brinker, C. J. *Proc. Natl. Acad. Sci. U.S.A.* **2012**, *109*, 17336−17341.
(7) Kresge, C. T.; Leonowicz, M. E.; Roth, W. J.; Vartuli, J. C.; Beck, J. S. *Nature* **1992**, *359*, 710−712.
(8) Bore, M. T.; Rathod, S. B.; Ward, T. L.; Datye, A. K. *Langmuir* **2003**, *19*, 256−264.
(9) Andersson, N.; Kronberg, B.; Corkery, R.; Alberius, P. *Langmuir* **2007**, *23*, 1459−1464.
(10) Carroll, N. J.; Pylypenko, S.; Atanassov, P. B.; Petsev, D. N. *Langmuir* **2009**, *25*, 13540−13544.
(11) Chen, S. H. *Annu. Rev. Phys. Chem.* **1986**, *37*, 351−399.
(12) Palmer, K. M.; Morse, D. C. *J. Chem. Phys.* **1996**, *105*, 11147.
(13) Petsev, D. N. In *Modern Aspects of Emulsion Science*; Binks, B. P., Ed.; Royal Society of Chemitsry: London, 1998.
(14) Kong, B.; Guan, B. H.; Yates, M. Z.; Wu, Z. B. *Langmuir* **2012**, *28*, 14137−14142.
(15) Li, W.; Xu, P.; Zhou, H. C.; Yang, L. R.; Liu, H. Z. *Sci. China−Technol. Sci.* **2012**, *55*, 387−416.
(16) Jones, B. H.; Lodge, T. P. *Polym. J.* **2012**, *44*, 131−146.
(17) Pylypenko, S.; Olson, T. S.; Carroll, N. J.; Petsev, D. N.; Atanassov, P. *J. Phys. Chem. C* **2010**, *114*, 4200−4207.
(18) Ashley, C. E.; Carnes, E. C.; Phillips, G. K.; Padilla, D.; Durfee, P. N.; Brown, P. A.; Hanna, T. N.; Liu, J. W.; Phillips, B.; Carter, M. B.; Carroll, N. J.; Jiang, X. M.; Dunphy, D. R.; Willman, C. L.; Petsev, D. N.; Evans, D. G.; Parikh, A. N.; Chackerian, B.; Wharton, W.; Peabody, D. S.; Brinker, C. J. *Nat. Mater.* **2011**, *10*, 389−397.
(19) Ashley, C. E.; Carnes, E. C.; Epler, K. E.; Padilla, D. P.; Phillips, G. K.; Castillo, R. E.; Wilkinson, D. C.; Wilkinson, B. S.; Burgard, C. A.; Kalinich, R. M.; Townson, J. L.; Chackerian, B.; Willman, C. L.; Peabody, D. S.; Wharton, W.; Brinker, C. J. *ACS Nano* **2012**, *6*, 2174−2188.
(20) Pylypenko, S.; Mukherjee, S.; Olson, T. S.; Atanassov, P. *Electrochim. Acta* **2008**, *53*, 7875−7883.
(21) Galeano, C.; Meier, J. C.; Peinecke, V.; Bongard, H.; Katsounaros, I.; Topalov, A. A.; Lu, A. H.; Mayrhofer, K. J. J.; Schuth, F. *J. Am. Chem. Soc.* **2012**, *134*, 20457−20465.
(22) Villermaux, E. *Annu. Rev. Fluid Mech.* **2007**, *39*, 419−446.
(23) Ahn, K.; Kerbage, C.; Hunt, T. P.; Westervelt, R. M.; Link, D. R.; Weitz, D. A. *Appl. Phys. Lett.* **2006**, *88*, 024104.
(24) Zhang, H.; Tumarkin, E.; Sullan, R. M. A.; Walker, G. C.; Kumacheva, E. *Macromol. Rapid Commun.* **2007**, *28*, 527−538.
(25) Duncanson, W. J.; Zieringer, M.; Wagner, O.; Wilking, J. N.; Abbaspourrad, A.; Haag, R.; Weitz, D. A. *Soft Matter* **2012**, *8*, 10636−10640.
(26) Vladisavljevic, G. T.; Henry, J. V.; Duncanson, W. J.; Shum, H. C.; Weitz, D. A. In *UK Colloids 2011*; London, July 4−6, 2011 Starov, V., Griffiths, P., Eds.; Royal Society of Chemistry: London, 2012; Vol. *139*, pp 111−114.
(27) Jurado, E.; Bravo, V.; Camacho, F.; Vicaria, J. M.; Fernandez-Arteaga, A. *Colloids Surf., A* **2007**, *295*, 91−98.
(28) Opedal, N. v. d. T.; Sorland, G.; Sjoblom. *J. Diffus. Fundam.* **2009**, *9*, 1−29.
(29) Mandal, A.; Samanta, A.; Bera, A.; Ojha, K. *Ind. Eng. Chem. Res.* **2010**, *49*, 12756−12761.
(30) Denkova, P. S.; Tcholakova, S.; Denkov, N. D.; Danov, K. D.; Campbell, B.; Shawl, C.; Kim, D. *Langmuir* **2004**, *20*, 11402−11413.
(31) Limpert, E.; Stahel, W. R.; Abbt, M. *Bioscience* **2001**, *51*, 341−352.
(32) Xia, Y. N.; Whitesides, G. M. *Annu. Rev. Mater. Sci.* **1998**, *28*, 153−184.
(33) Anna, S. L.; Bontoux, N.; Stone, H. A. *Appl. Phys. Lett.* **2003**, *82*, 364−366.
(34) Aveyard, R.; Binks, B. P.; Clark, S.; Mead, J. *J. Chem. Soc., Faraday Trans. I* **1986**, *82*, 125−142.
(35) Duclaux, V.; Clanet, C.; Quere, D. *J. Fluid Mech.* **2006**, *556*, 217−226.
(36) Carroll, N. J.; Rathod, S. B.; Derbins, E.; Mendez, S.; Weitz, D. A.; Petsev, D. N. *Langmuir* **2008**, *24*, 658−661.
(37) Aranberri, I.; Beverley, K. J.; Binks, B. P.; Clint, J. H.; Fletcher, P. D. L. *Langmuir* **2002**, *18*, 3471−3475.